Journal of Ovonic Research Vol. 20, No. 6, November - December 2024, p. 889 - 896

Structural simulation and preparation of graphite with phosphate intercalation

Y. Xing, Y. Zhou*
College of Materials Science and Engineering, Nanjing Tech University, South PuZhu Road No.30, Nanjing, 211816, PR-China

This study introduces a novel method for synthesizing phosphate-intercalated graphite (G-PO_4^{3-}-G) using electrochemical techniques with oxidation-based pretreatment. Employing CP2K software for first-principles calculations, the research demonstrates successful creation of G-PO_4^{3-}-G, characterized by an enhanced, stable crystal structure. Techniques such as XRD, SEM with EDS mapping, and TEM verify the effective intercalation of phosphate ions, significantly boosting the material's hydrogen storage capabilities.

(Received April 25, 2024; Accepted December 23, 2024)

Keywords: Hydrogen storage, Phosphate-intercalated graphite, CP2K

1. Introduction

Amid the ongoing transformation of the global energy landscape and the push for enhanced environmental governance, the quest for efficient and environmentally friendly energy storage materials has taken center stage in scientific inquiry. Hydrogen energy, celebrated for its high energy density, emission-free combustion, and versatile sourcing, has emerged as a focal point of interest. Nonetheless, unresolved safety and economic challenges continue to hamper the broader adoption of hydrogen storage technologies.

The method of physical adsorption for hydrogen storage necessitates materials endowed with a substantial specific surface area, thereby providing a plethora of sites for hydrogen storage. Graphite, with its distinctive two-dimensional structure, expansive surface area, and superior physicochemical attributes, has garnered significant interest as a prime candidate for hydrogen adsorption.

Recent advancements have seen a surge in research aimed at enhancing graphite's hydrogen storage capabilities through various modifications. These efforts predominantly focus on augmenting its storage capacity via chemical adjustments or the creation of composite materials. Notably, the incorporation of alkali metals[1-7], alkaline earth metals[6, 8-11], and transition metals atoms[12-20] into graphite has demonstrated promising results. Pioneering work in this area includes the utilization of Density Functional Theory (DFT) by Cabria[5] and colleagues to model lithium-modified graphite (Li-Graphite), which exhibited a notable increase in H2 adsorption capacity. Similarly, research[8] utilizing the VASP software package identified optimal adsorption

* Corresponding author: yongminzhou@nitech.edu.cn
https://doi.org/10.15251/JOR.2024.206.889

sites for Li atoms on graphite, further corroborating the potential for enhanced hydrogen storage.

Moreover, modifications to graphite's electronic structure and chemical affinity through the introduction of functional groups or element doping have shown to bolster its hydrogen adsorption capacity and structural stability. For example[21], the preparation of Ni and B doped graphite (Ni/B@Graphite) and subsequent hydrogen storage experiments highlighted the material's capacity to absorb 2.81wt.% of H2 under specific conditions. Such modifications not only enhance graphite's affinity for hydrogen but also mitigate the agglomeration of modifier atoms, primarily through the induction of new electronic states conducive to H_2 storage.

In addition to chemical modifications, physical alterations such as adjusting graphite's interlayer distance or incorporating porous structures have also proven effective in improving hydrogen storage performance[22]. However, despite theoretical advancements promising significant hydrogen storage capacities, empirical achievements have fallen short of expectations. Investigations have revealed that even optimally prepared hydrogen storage materials have yet to attain the theoretical storage capacities when tested under practical conditions. This discrepancy underscores the limitations of current theoretical models in accurately reflecting real-world outcomes.

2. Simulation and experimentation

2.1. Simulation details

First-principles calculations on the structure of phosphate intercalated graphite (G-PO_4^{3-}-G) were conducted using the QUICKSTEP module within the CP2K[23] software suite. A periodic boundary condition was implemented to mitigate interactions among multi-layered graphite sheets, incorporating a vacuum buffer of 20.0 Å to ensure isolation. The Brillouin zone was sampled at a k-point grid of 4x4x1. Geometric optimisation employed the BFGS algorithm, constraining each atom to a maximum force of 0.02 eV/Å and a maximum displacement of 0.003 Å. A cutoff energy of 600 Ry and a self-consistent field (SCF) convergence criterion of 1*10-6 a.u. were set. The Grimme D3 empirical dispersion correction was employed to accurately modeling weak intermolecular interactions. To simplify the electronic complexity of the periodic systems and enhance computational efficacy, Goedecker-Teter-Hutter (GTH) [24] pseudopotentials were applied. The exchange-correlation energy of electrons was determined using the Perdew-Burke-Ernzerhof (PBE) function within the Generalized Gradient Approximation (GGA) framework. The accuracy of computed molecular energies was further refined by including polarization functions via the polarized DZVP[25] Gaussian basis set. The predetermined interlayer distance in graphite was adjusted to 5 Å to facilitate convergence during geometric optimisation.

2.2. Preparation of graphite with phosphate intercalation

In this paper, a series of orthogonal as well as one-way experiments were carried out in order to select the optimal concentration for the preparation of G-PO_4^{3-}-G. G-PO_4^{3-}-G was achieved via an electrochemical method preceded by a pretreatment process. The preparation comprised two main steps: initially, the graphite electrode underwent pretreatment by immersion in a potassium

permanganate solution of predetermined concentration, followed by cleaning and drying with deionised water after the pretreatment conditions were met. Subsequently, in the electrochemical electrolysis phase, the pretreated graphite electrode served as the anode, with the electrolysis conducted under preset conditions before cleaning, drying, and performance evaluation. The pretreatment utilized a 0.1 M potassium permanganate solution, maintained at 60℃ using a water bath. The electrolysis employed a 3.0 M phosphoric acid solution, with a set voltage of 3.0 V and duration of 3 hours.

2.3. Characterization of G-PO_4^{3-}-G

The interplanar spacing of G-PO_4^{3-}-G was characterised using a Bruker D8 Advance X-ray Diffractometer, spanning a scanning range of 20–60°(2θ) with Cu Kα1 radiation at a wavelength of 1.5406 Å and a rate of 0.05 s^{-1}. A Regulus8100 instrument, equipped for scanning electron microscopy (SEM) with energy dispersive X-ray analysis, was utilized at accelerating voltages of 5 and 30 kV. Transmission electron microscopy (TEM) examinations were performed with a FEI Tecnai G2 F20, operating at 200 kV.

3. Results and discussion

3.1. Structural simulation results

As illustrated in Fig 1, the lattice constants for G-PO_4^{3-}-G were determined as a=12.3386 Å, b=12.3386 Å, and c=30.0000 Å. Notably, the interlayer spacing at phosphorus atom sites between the dual layers of graphite measures were found to be 7.48 Å, with the boundary of the supercell exhibiting a spacing of 7.22 Å. This represents a considerable expansion along the c-axis and an increased interlayer distance compared to the pre-optimisation measurements of intrinsic bilayer graphite (a=12.299995 Å, b=12.299995 Å, c=13.600 Å), which were previously 3.35 Å.

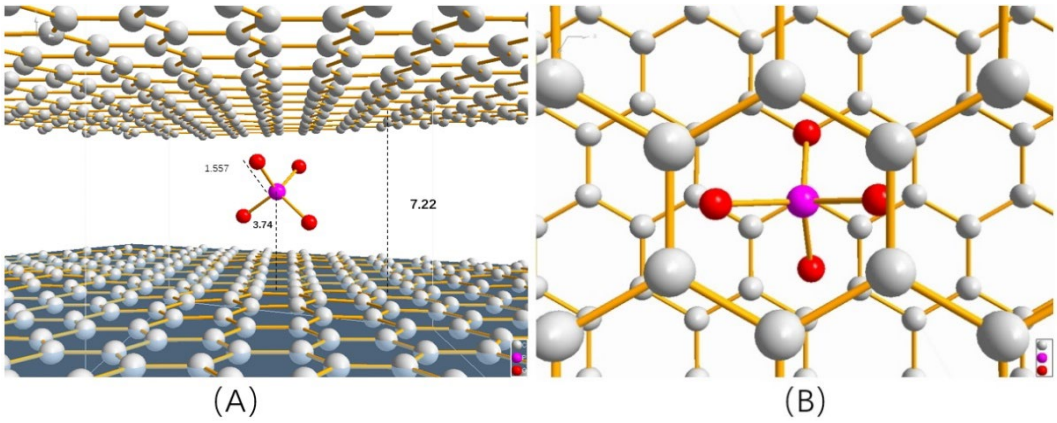

Fig. 1. Illustrates the supercell structure of phosphate-intercalated graphite (G-PO_4^{3-}-G). (a) provides a view along the crystallographic a-axis, while (a) depicts the view along the c-axis. In the diagram, carbon atoms are denoted by grey spheres, phosphorus atoms by pink spheres, and oxygen atoms by red spheres, with spatial measurements in Å.

Prior to optimisation, the phosphate ion bond lengths uniformly measured 1.840 Å, with a bond angle of 109.471°. Optimisation led to varying contractions in these bond lengths 1.5570 Å, 1.5670 Å, 1.5660 Å, and 1.5610 Å with corresponding bond angles adjusting to 108.256°, 110.986°, 107.332°, 109.969°, 109.710°, and 110.588°, respectively. Although the bond angles remained relatively stable, the bond lengths decreased by approximately 0.3 Å. The phosphorus atoms are situated about 3.74 Å from both the upper and lower graphite layers, with the carbon atoms in the vicinity of the phosphate ions showing angles between 119.8° and 120.3°. The C-C bond lengths ranged between 1.42 Å and 1.43 Å, closely aligning with the intrinsic graphite's parameters. Calculation of the G-PO_4^{3-}-G model obtained from the structural simulation shows that the XRD diffraction spectrum corresponding to this crystal structure has the strongest diffraction peak corresponding to the (004) crystal plane, which corresponds to a 2θ of 12.8°.

The interlayer modification by phosphate group intercalation results in altered spacing without significantly impacting the hexagonal honeycomb structure of graphite, thereby preserving its structural integrity. The introduction of these molecules between the graphite layers transforms its original stacked two-dimensional structure into a three-dimensional sandwich-like configuration. Regions of graphite with inserted phosphate groups develop noticeable protrusions, creating cage-like structures that enhance the material's specific surface area, which is advantageous for hydrogen storage.

3.2. X-ray diffraction (XRD) analysis

XRD analysis conducted on the G-PO_4^{3-}-G sample and graphite raw materials, as demonstrated in Fig. 2, identifies the characteristic peak of graphite (002) surface. Two novel characteristic peaks, P1 and P2, were observed in G-PO_4^{3-}-G. Peak P1, situated near 24.2°, are absent in graphite raw materials and Peak P2, located approximately 0.8° (27.34° 2θ) to the right of the standard graphite (002) crystal face peak (26.54°).

Despite fluctuations in intensity and location under varying experimental conditions, Peaks P1 and P2 consistently emerge at identical positions. The spacing for crystal planes P1 and P2 in G-PO_4^{3-}-G measures at 3.672 Å and 3.322 Å, respectively. Remarkably, P2 aligns closely with the graphite (002) crystal face distance (3.35 Å), and its prominence among all observed peaks suggests a shift from the original graphite (002) peak position. Conversely, P1 is indicative of intercalation products. The smoother spectrum of G-PO_4^{3-}-G, in comparison to raw graphite, signals enhanced crystallinity.

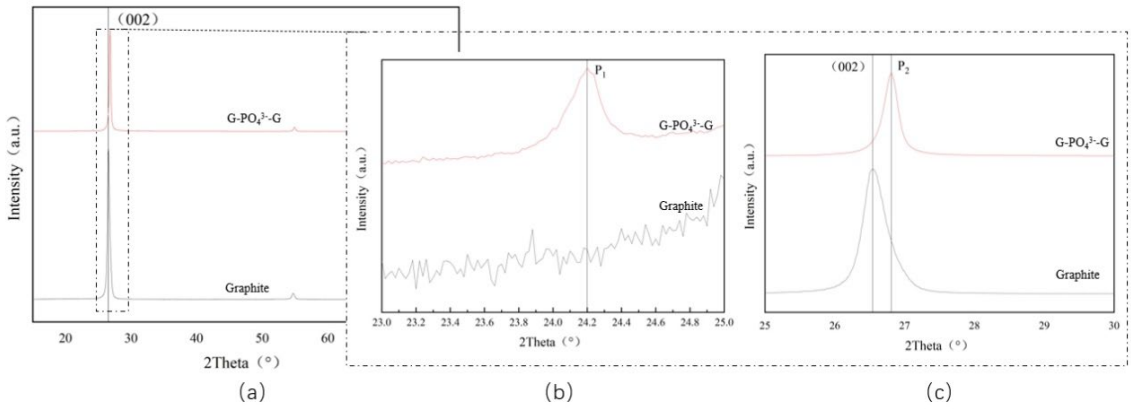

Fig. 2. XRD patterns of G-PO_4^{3-}-G and Graphite raw materials (a) in the range of 15 to 80° and (b). in the range of 23 to 25° (c) in the range of 25 to 30°.

3.3. SEM and EDS mapping characterization results

Fig. 3 displays the SEM images and EDS mapping results for G-PO43--G, as can be seen from the figure, graphite with smooth surface has a lower concentration of phosphorus, while graphite with many surface folds has a higher phosphorus content. This phenomenon is attributed to the substantial presence of phosphate ions within the intercalation layer, resulting in areas of elevated phosphorus concentration, which are more uniformly distributed across the morphology. The EDS spectrum of G-PO43--G, also presented in Fig. 4, reveals a phosphorus to oxygen mass ratio of approximately 1:2. This ratio suggests a coherent intercalated structure, with the excess oxygen likely introduced during the pretreatment phase by the potassium permanganate solution.

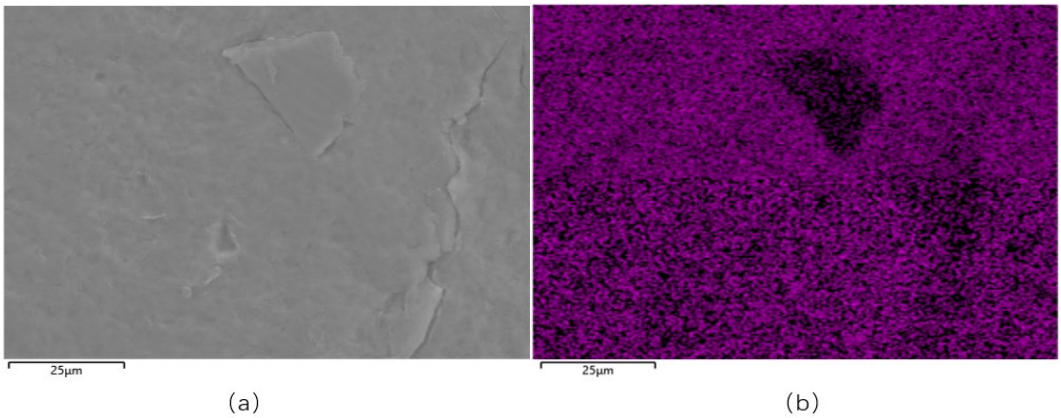

Fig. 3. SEM photo as well as EDS mapping of G-PO_4^{3-}-G, Fig. (a) SEM photo, Fig. (b) EDS mapping of phosphorus elements.

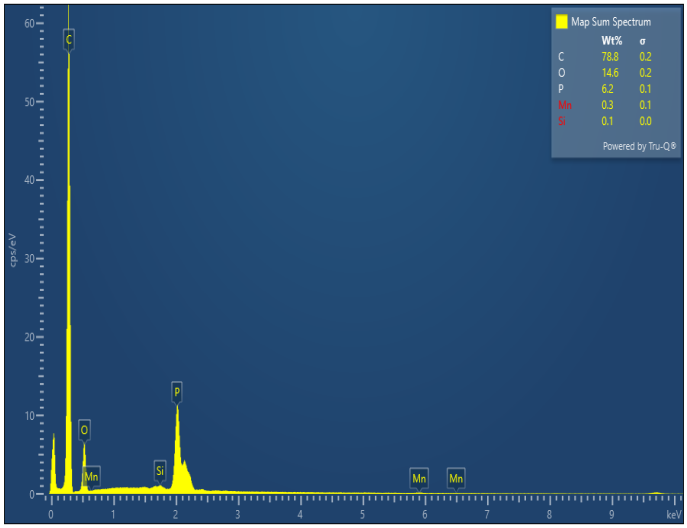

Fig. 4. EDS spectra of G-PO_4^{3-}-G.

3.4. TEM analysis

Fig. 5 delineates the TEM analysis outcomes for G-PO_4^{3-}-G. Panel (a) of Fig. 5 showcases clear lattice fringes with the delineated region spanning 3.406 nm, hosting nine peaks that yield an average inter-peak distance of 0.379 Å. Panel (b) depicts the HETEN spectrum, illustrating two sets of mixed peaks, varying in intensity but within a similar range, accompanied by a cross-arrangement pattern. These observations align with the XRD analysis, which identifies two distinct peaks characteristic of the G-PO_4^{3-}-G sample.

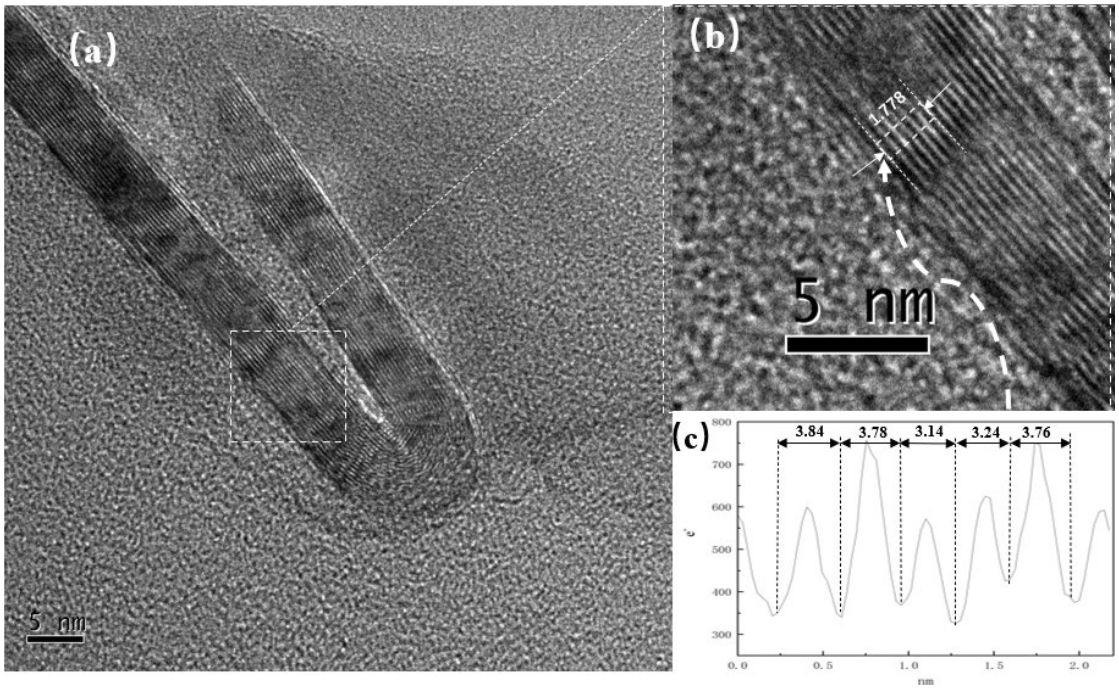

Fig. 5 (a) HRTEM image of G-PO_4^{3-}-G, (b) Magnified view of the boxed region in (a), (c) HRTEM liner intensity of the boxed region in (b).

4. Conclusion

G-PO_4^{3-}-G was achieved through an electrochemical method, enhanced by an oxidation-based pretreatment. First-principles analysis, conducted using CP2K software, aligned theoretical predictions with experimental observations, demonstrating the synthesis of G-PO_4^{3-}-G with a stable and refined crystal structure. Transmission Electron Microscopy (TEM) High-Energy Electron Transmitted (HETEN) spectrum, in conjunction with X-ray Diffraction (XRD) findings, unveiled new crystalline structures, albeit with varying uniformity. A notable discrepancy between the XRD characterisation and simulation outcomes stems from the initial assumption of a bilayer structure in simulations, whereas actual G-PO_4^{3-}-G samples exhibited multilayer stacking.

This divergence highlights the challenges in achieving uniform phosphate ion intercalation and the limitations of intercalation quantity. Nevertheless, TEM and XRD analyses confirmed that phosphate ion intercalation modifies the crystal structure of graphite. Specifically, the interlayer spacing at intercalation sites increases, leading to a reduction in the surrounding graphite layer spacing. This effect, evidenced by the rightward shift of the characteristic peak P2 in XRD and the presence of undulating lattice fringes in TEM images, illustrates varied layer spacings within the stacked structure. The differences between the simulated and observed crystal structures emphasize the imperative for model refinement and production enhancement of G-PO_4^{3-}-G. This research serves as a foundation for advancing novel hydrogen storage materials and signifies the inaugural synthesis of this compound, as reported in this study.

References

[1] F. D. Wang, F. Wang, N. N. Zhang, Y. H. Li, S. W. Tang, H. Sun, Y. F. Chang, R. S. Wang, Chemical Physics Letters,555(Complete), 212, (2013); https://doi.org/10.1016/j.cplett.2012.11.015

[2] T. Hussain, A. D. Sarkar, R. Ahuja, Applied Physics Letters, 101(10), 968, (2012); https://doi.org/10.1063/1.4751249

[3] M. Shadman, S. Yeganegi, M. R. Galugahi, Journal of the Iranian Chemical Society, (2015); https://doi.org/10.1007/s13738-015-0728-3

[4] C. Ataca, E. Akturk, S. Ciraci, H. Ustunel, Applied Physics Letters, 93(4), 043123, (2009); https://doi.org/10.1063/1.2963976

[5] I. Cabria, M. J. Lopez, J. A. Alonso, Journal of Chemical Physics,128(14), 24, (2008); https://doi.org/10.1063/1.2900964

[6] Adolfo, Ferre-Vilaplana, The Journal of Physical Chemistry C,112(10), 3998, (2008); https://doi.org/10.1021/jp0768874

[7] S. Seenithurai, R. K. Pandyan, S. V. Kumar, C. Saranya, M. Mahendran, International Journal of Hydrogen Energy,39(21), 11016, (2014); https://doi.org/10.1016/j.ijhydene.2014.05.068

[8] C. Ataca, E. Akturk, S. Ciraci, Hydrogen storage of calcium atoms adsorbed on graphene: First-principles plane wave calculations.

[9] S. L. Er, G. A. De Wijs, G. Brocks, Journal of Physical Chemistry C,113(43), 18962, (2009); https://doi.org/10.1021/jp9077079

[10] T. Hussain, Applied Physics Letters,100(18), 302, (2012); https://doi.org/10.1063/1.4710526

[11] C. Chen, J. Zhang, B. Zhang, H. M. Duan, Journal of Physical Chemistry C,117(9), 4337, (2013); https://doi.org/10.1021/jp308271b

[12] E. Durgun, S. Ciraci, T. Yildirim, Physical review,77(8), 672, (2008); https://doi.org/10.1103/PhysRevB.77.085405

[13] H. P. Zhang, X. G. Luo, X. Y. Lin, X. Lu, Y. Leng, International Journal of Hydrogen Energy,38(33), 14269, (2013); https://doi.org/10.1016/j.ijhydene.2013.07.098

[14] S. A. Shevlin, Z. X. Guo, Journal of Physical Chemistry C,112(44), 17456, (2010); https://doi.org/10.1021/jp800074n

[15] E., Durgun, S., Ciraci, W., Zhou, T., Yildirim, Physical Review Letters,97(22), 226102, (2006); https://doi.org/10.1103/PhysRevLett.97.226102

[16] Seul-Yi, Lee, Soo-Jin, Park, Journal of nanoscience and nanotechnology, (2013).

[17] Y. Liu, L. Ren, Y. He, H. P. Cheng, Journal of Physics Condensed Matter,22(44), 445301, (2010); https://doi.org/10.1088/0953-8984/22/44/445301

[18] G. M. Psofogiannakis, G. E. Froudakis, Chemical Communications,47(28), 7933, (2011); https://doi.org/10.1039/c1cc11389e

[19] T. Mashoff, M. Takamura, S. Tanabe, H. Hibino, S. Heun, Applied Physics Letters,103(1), 013903 (4 pp.), (2013); https://doi.org/10.1063/1.4812830

[20] B. P. Vinayan, K. Sethupathi, S. Ramaprabhu, Journal of Nanoscience and Nanotechnology,12(8), 6608, (2012); https://doi.org/10.1166/jnn.2012.4539

[21] Y. Wang, J. Liu, K. Wang, T. Chen, X. Tan, C. M. Li, International Journal of Hydrogen Energy,36(20), 12950, (2011); https://doi.org/10.1016/j.ijhydene.2011.07.034

[22] V. B. Parambhath, R. Nagar, K. Sethupathi, S. Ramaprabhu, Journal of Physical Chemistry C,115, 15679, (2011); https://doi.org/10.1021/jp202797q

[23] T. D. Kühne, M. Iannuzzi, M. D. Ben, V. V. Rybkin, J. Hutter, CP2K: An Electronic Structure and Molecular Dynamics Software Package I. Quickstep: Efficient and Accurate Electronic Structure Calculations, (2020); https://doi.org/10.1063/5.0007045

[24] J. Vandevondele, J. Hutter, Journal of Chemical Physics,127(11), 4365, (2007); https://doi.org/10.1063/1.2770708

[25] C. Hartwigsen, S. Goedecker, J. Hutter, Physical Review B,58(7), 3641, (1998); https://doi.org/10.1103/PhysRevB.58.3641